# Angle-resolved photoemission spectroscopy view on the nature of Ce 4$f$ electrons in the antiferromagnetic Kondo lattice $CePd_5Al_2$

Ya-Hua Yuan,[1,*] Yu-Xia Duan,[1,*] Ján Rusz,[2] Chen Zhang,[1] Jiao-Jiao Song,[1] Qi-Yi Wu,[1] Yasmine Sassa,[2,3] Oscar Tjernberg,[4] Martin Månsson,[4] Magnus H. Berntsen,[4] Fan-Ying Wu,[1] Shu-Yu Liu,[1] Hao Liu,[1] Shuang-Xing Zhu,[1] Zi-Teng Liu,[1] Yin-Zou Zhao,[1] P. H. Tobash,[5] Eric D. Bauer,[5] Joe D. Thompson,[5] Peter M. Oppeneer,[2] Tomasz Durakiewicz,[6] and Jian-Qiao Meng[1,†]

[1]*School of Physics and Electronics, Central South University, Changsha 410083, Hunan, People's Republic of China*
[2]*Department of Physics and Astronomy, Uppsala University, Box 516, S-75120 Uppsala, Sweden*
[3]*Department of Physics, Chalmers University of Technology, S-41296 Göteborg, Sweden*
[4]*Department of Applied Physics, KTH Royal Institute of Technology, Electrum 229, S-16440, Stockholm, Kista, Sweden*
[5]*Los Alamos National Laboratory, Los Alamos, New Mexico 87545, USA*
[6]*Institute of Physics, Maria Curie Sklodowska University, 20-031 Lublin, Poland*

(Received 16 November 2020; revised 3 February 2021; accepted 2 March 2021; published 11 March 2021)

We report an angle-resolved photoemission spectroscopy study of the antiferromagnetic Kondo lattice $CePd_5Al_2$, focusing on the quasi-two-dimensional $k$-space nature of its Fermi surface and, tuning photon energy to the Ce 4$d$–4$f$ on-resonance transition, the hybridization of the Ce 4$f$ state. A strong shoulder feature on the $f^0$ peak was detected, suggesting hybridization between conduction and $f$ bands. On-resonance spectra revealed narrow, yet hybridized quasiparticle bands with sharp peaks and $\sim$ 9 meV energy dispersion near the Fermi energy $E_F$. The observed dispersive hybridized $f$ band can be well described by a hybridization-band picture based on the periodic Anderson model (PAM). Hence, the 4$f$ electrons in $CePd_5Al_2$ display a dual nature, with both localized and itinerant features, but with dominantly localized character.

DOI: 10.1103/PhysRevB.103.125122

Heavy fermion (HF) compounds have been studied extensively for their rich physical properties since being discovered in 1975 [1]. Hybridization between itinerant conduction band electrons and localized $f$ electrons ($c$–$f$) plays a key role for several unique quantum states and quantum phase transitions, including unconventional superconductivity [2], quantum criticality [3], antiferromagnetism [4], non-Fermi Liquid [5], possible Weyl fermion [6,7], and topological nodal-line semimetal [8]. Many isostructural compounds $RPd_5Al_2$ ($R$ = U, Ce, Y, Pr, Nd, Sm, Gd) have been successfully synthesized [9–13] since the neptunium-based HF superconductor $NpPd_5Al_2$ was first discovered in 2007 [9]. These series of HF compounds have a common tetragonal $ZrNi_2Al_5$-type structure with the space group $I4/mmm$, in which the $RPd_3$ and $Pd_2Al_2$ layers are stacked along its $c$ axis. Several studies suggest that, except for the Y, Pr, and U compounds [10], most of the family members undergo antiferromagnetic (AFM) phase transitions at low temperature [9–13]. $PrPd_5Al_2$ compounds have a singlet ground state [11], and $UPd_5Al_2$ is a paramagnet [10].

$CePd_5Al_2$ has lattice parameters: $a = 4.156$; $c = 14.883$ Å. It undergoes two magnetic transitions at $T_{N1} = 3.9$ K (or 4.1 K) and $T_{N2} = 2.9$ K [12–15]. Unlike $NpPd_5Al_2$, which exhibits superconductivity near its AFM ordering ($T_c$ = 4.9 K) at ambient pressure [9], bulk superconductivity of $CePd_5Al_2$ was induced by pressurization in the region of 9–12 GPa wherein it reached a maximum $T_c = 0.57$ K [13]. An intermediate Sommerfeld coefficient $\gamma$, 60 mJ/(mol K$^2$) for polycrystal [12] or 18 mJ/(mol K$^2$) for single crystal [16]], was estimated by specific heat experiments. This is greater than that of uncorrelated metals [$\sim$ 10 mJ/(mol K$^2$)] and less than that of typical HF compounds [$\sim$ 400 mJ/(mol K$^2$)]. This suggests that $CePd_5Al_2$ cannot be considered as a conventional HF compound. Ce 4$f$ electrons are considered to be localized due to the small Sommerfeld coefficient $\gamma$ [16]. Specific heat experiments suggested that the $Ce^{3+}$ ion crystalline electric field (CEF) ground state is a Kramers doublet of well-localized 4$f$ electron [13,16,17]. Inelastic neutron scattering measurements on a powder sample showed CEF excitations at 21.3 and 22.4 meV [15]. Single-crystal neutron diffraction observed an in-plane modulated magnetic structure [Q = (0.235, 0.235, 0)] below $T_{N1}$ [14,15]. Resistivity measurements indicated the presence of Kondo lattice and Fermi-Liquid behavior [12].

The electronic structure of $CePd_5Al_2$ appears to have quasi-two-dimensional (2D) characteristics [13] due to its layered structure and large interlayer distance. This is unusual in HF materials. We present the first angle-resolved photoemission spectroscopy (ARPES) data on this compound, utilizing tunable photon energies with high energy and momentum resolution on high-quality single crystals of $CePd_5Al_2$. Varying systematically the photon energies, we mapped the 3D Fermi surface (FS) of $CePd_5Al_2$ along the $k_z$ (perpendicular) direction. The FS topology is compared to density-function

*These authors contributed equally to this work.
†Corresponding author: jqmeng@csu.edu.cn

 

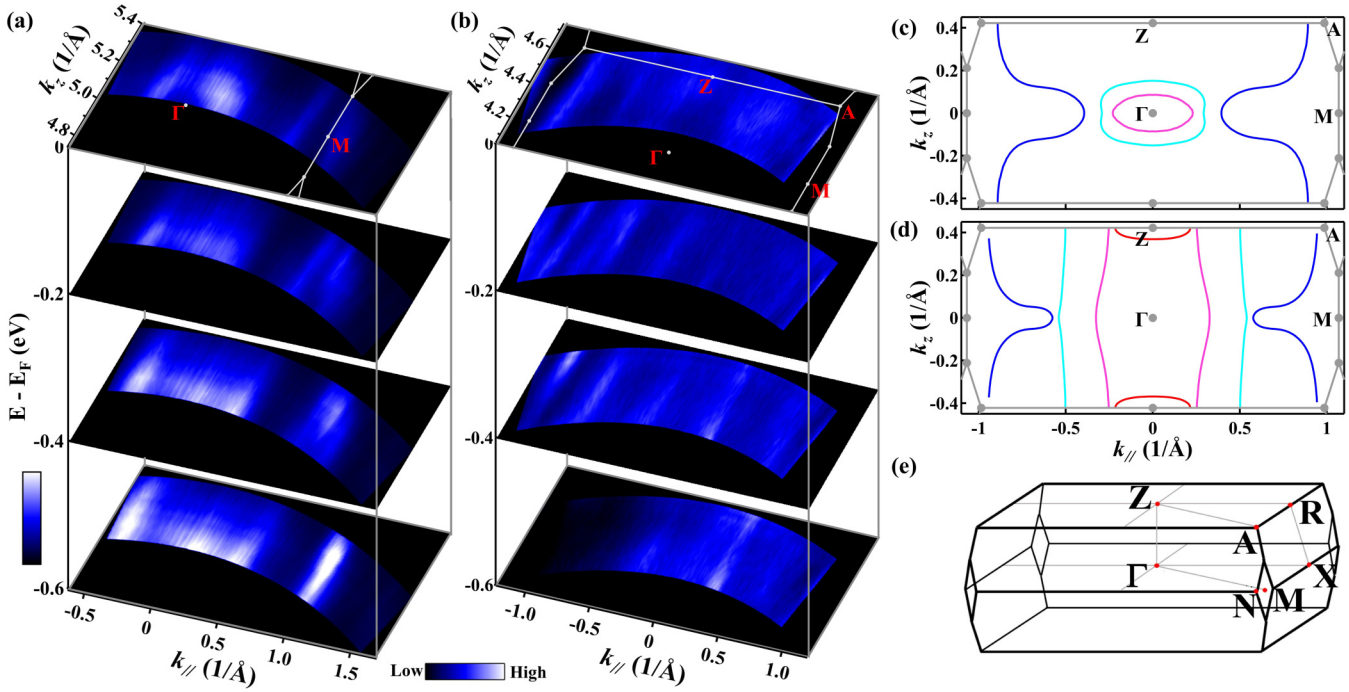


FIG. 1. (**a**) and (**b**) Experimental 3D FS maps constructed cuts along $k_z$ in the Γ-M-A-Z plane and measured with $h\nu = 87$–$100$ and $h\nu = 61$–$74$ eV phonons, respectively. Band structure constant-energy contours are at $E_F$ and at 200, 400, and 600 meV below $E_F$, integrated over 20 meV. (**c**) and (**d**) DFT-calculated Fermi contours in the Γ-M-A-Z plane for $CePd_5Al_2$ and $LaPd_5Al_2$, respectively. (**e**) The 3D BZ of $CePd_5Al_2$ with high-symmetry momentum points marked.

theory (DFT) calculations. On-resonance $4d-4f$ ARPES is measured to study the nature of Ce $4f$ electrons.

Single crystals of $CePd_5Al_2$ were prepared by arc-melting stoichiometric amounts of the elements on a water-cooled copper hearth under a UHP argon atmosphere. The $CePd_5Al_2$ boule was crushed and small single crystals were extracted. ARPES measurements were carried out with VG-SCIENTA R4000 detectors at the SIS X09LA beamline of the Swiss Light Source. All samples were cleaved *in situ* along the (001) axis and measured in an ultrahigh vacuum with a base pressure better than $4 \times 10^{-11}$ mbar. ARPES data were collected at $T = 10$ K, which is above the AFM transition temperature $T_{N1}$. An angular resolution of 0.2° was used for all measurements.

We used photon energy-dependent measurement to detect the $k_z$ dispersion in the high-symmetry Γ-M-A-Z plane to verify $CePd_5Al_2$ electronic structure dimensionality. The $k_z$ dispersions are shown in Figs. 1(a) and 1(b) using a reasonable value for the inner potential $V_0$ of 16 eV. Data were collected using two different photon energy ranges 87–100 and 61–74 eV, covering half a Brillouin zone (BZ) and including both Γ and Z points. The Fermi sheets show overall quasi-2D characters even though the shape and intensity of part of the Fermi sheets changed with photon energy (see Fig. S1 of the Supplemental Material [18] for more details). The near $E_F$ spectrum is greatly affected by the heavy $f$ electron, which prevents clear FS detection. Weak $k_z$ dispersion prevents an exact determination of the inner potential $V_0$. Figs. 1(c) and 1(d) display the calculated FS topologies of $CePd_5Al_2$ and $LaPd_5Al_2$, respectively. The $LaPd_5Al_2$ band structure is calculated using the same lattice parameters as $CePd_5Al_2$, where only the $4f$ occupation is varied. $LaPd_5Al_2$ is a $4f^0$ rare-earth system with $3^+$ valence. Itinerant and localized model calculations suggest different electronic structures along Γ-M. Both of these calculations are somewhat consistent with some of the experimental results, and some calculated dispersions were not observed in the data.

ARPES measurements were performed at the Ce $4d$–$4f$ transition to enhance the $f$-electron spectral weight near $E_F$ by tuning the photon energies to 123 eV. Figure 2(a) shows the on-resonance spectra of $CePd_5Al_2$. Figures 2(b) and 2(c) show the angle-resolved and angle-integrated photoemission spectroscopy of the intensity plot in Fig. 2(a), respectively. The high-intensity, dispersionless $f^0$ state is around $-1.63$ eV. This value is higher than that of other Ce-based HF compounds. For example, it is $-2.5$ eV for $CePt_2In_7$ [19], $-2.3$ eV for $CeIrIn_5$ [20], $-2$ eV for $CeIn_3$ [21], and $-1.9$ eV for $CeRh_2Si_2$ [22]. This flat band is generated by the pure charge excitations of the trivalent Ce ion ($4f^1 \rightarrow 4f^0$); it is commonly called the "ionization peak" [23]. In Figs. 2(a) and 2(b), slightly above the $f^0$ state, a weaker nondispersive structure was observed at around $-1.3$ eV. A shoulder appears at the front edge of the huge $f^0$ peak. It is indicated by the arrow in Fig. 2(c). The calculation suggests that the valence band does not have a flat band around this energy. Such a shoulder of the $f^0$ peak probably originates from hybridization spreading [21,22].

The Ce $4f$ character is strongly enhanced, as demonstrated by the heavy quasiparticle bands ($f^1$ state) close to $E_F$ [Fig. 2(c)]. Spin-orbit splitting results in an $f^1$ state that splits into two sharp peaks, $f^1_{7/2}$ and $f^1_{5/2}$. The $f^1_{7/2}$ state is

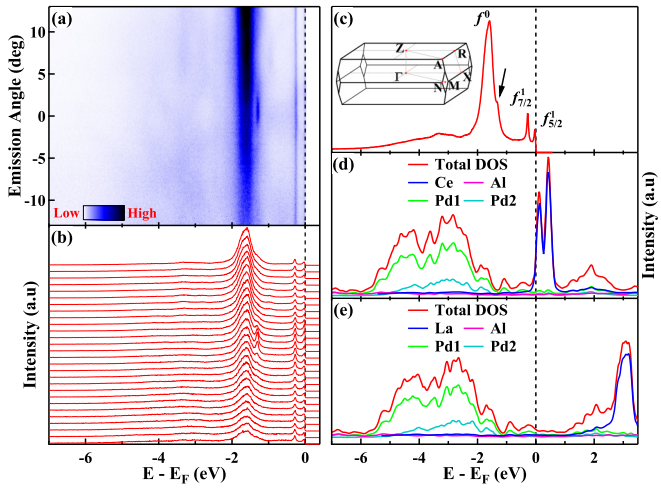


FIG. 2. (**a**) Raw data of a 2D image showing the on-resonance valence band structure for $CePd_5Al_2$. The total energy resolution was set at $\sim$ 30 meV. (**b**) Photoemission spectra EDCs corresponding to (a). (**c**) Angle-integrated photoemission spectroscopy of the intensity plot in (a). Inset: A 3D BZ zone with high-symmetry momentum points marked. Γ, $M$, $N$, and $X$ are at the $k_z = 0$ plane while $Z$, $A$, and $R$ points are at the $k_z = 2\pi/c$ plane. (**d**) Calculated Ce $4f$, Pd $3d$, and Al $3p$ DOS vs. energy $E$ for $CePd_5Al_2$. (**e**) The calculated DOS of $CePd_5Al_2$'s isostructural compound $LaPd_5Al_2$.

located at $\sim$280 meV below $E_F$. The $f^1_{5/2}$ state is located near $E_F$. These characteristic features are widely founded in Ce-based HF compounds [19–26]. The $4f^1$ state intensity is much weaker than that of other itinerant $f$-electron HF compounds such as $URu_2Si_2$ [27,28]. It is stronger than that of partially itinerant $f$-electron HF compounds such as $CePt_2In_7$ [19]. According to the single-impurity Anderson model, it is widely accepted that the $f^1$-to-$f^0$ intensity ratio, $[I(f^1_{7/2})+I(f^1_{5/2})]/I(f^0)$, can reflect the hybridization strength. The $CePd_5Al_2$ $f^1$-to-$f^0$ intensity ratio is about 0.11 (see Fig. S2 of the Supplemental Material [18] for more details). It is stronger than that of $CePt_2In_7$ [19] and much weaker than that of Ce$M$In$_5$ [20,24]. It can be deduced that $CePd_5Al_2$ hybridization strength is stronger than that of $CePt_2In_7$ and weaker than that of Ce$M$In$_5$.

Figures 2(d) and 2(e) display comparisons of the calculated density of states (DOS) of the isostructural compounds $CePd_5Al_2$ and $LaPd_5Al_2$, respectively. DFT calculations suggest that, unlike $LaPd_5Al_2$, where the La $4f$ electrons are well above $E_F$, the Ce $4f$ electrons in $CePd_5Al_2$ are mostly located just about 0.1 eV above $E_F$, and a small amount of Ce $4f$ electrons appears below $E_F$. The feature close to $E_F$ is considered to originate from the tail of the Kondo resonance peak above $E_F$.

A comparison of spectra, dominated by $d$-band spectral weight with spectra having Ce $4f$ weight resonantly enhanced, provides insight in the basic localization or itinerant properties of the $4f$ electrons. The three spectra ranges from off- to on-resonance are shown in Fig. 3. Close to $E_F$, the off-resonance spectrum ($h\nu = 115$ eV) shows a DOS of non-$f$ orbital character dominated by Pd $4d$ states [Fig. 3(a)]. The conduction band intensity is weak, possibly due to the emission from Pd $4d$ state which is strongly suppressed by the Cooper minimum around 115 eV [29]. Dominant Pd $4d$ emission in the off-resonance spectrum is replaced by the Ce $4f$ emission in the on-resonance spectrum as photon energy changes [Fig. 3(c)]. A Fano resonance enhancement of the Ce $4f$ emission at 123 eV photon energy reveals an on-resonance spectrum which shows a gathering of Ce $4f$ spectra weight near $E_F$. The intense $4f$ character near $E_F$ is seen in the angle-integrated spectra [Fig. 3(d)]. Two flat quasiparticle bands, $f^1_{7/2}$ and $f^1_{5/2}$ state, formed by spin-orbital spitting, appear just below $E_F$. The nonresonance spectrum can also distinguish two Kondo resonance peaks having very weak intensity. They originate from the Ce $4f$ electrons. The intensity of the two flat bands shows an obvious momentum dependence. Flat band spectral weight is markedly stronger around the $f$ and conduction band intersection than that of other positions. The $f^1_{5/2}$ state strength is much weaker than that of $f^1_{7/2}$ suggesting that hybridization is weaker [30].

When hybridization occurs, in addition to the redistribution of the $f$-electron spectrum weight, a dispersive heavy quasiparticle band should be observed around the intersection of

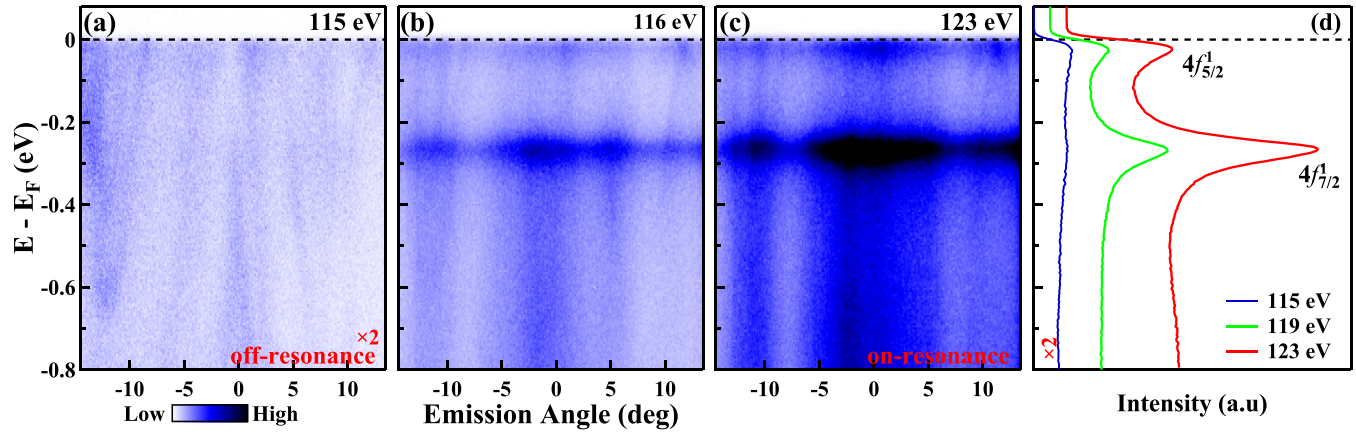


FIG. 3. (**a**)–(**c**) Raw band maps of $CePd_5Al_2$ along M'-Γ''-M' directions taken at photon energies of 115, 119, and 123 eV, respectively. This set of data shows the evolution of momentum-resolved Ce $4f$ emissions across the Ce $4d$–$4f$ threshold. (**d**) The angle-integrated EDCs for data in (a)–(c). The positions of the $f^1_{5/2}$ and $f^1_{7/2}$ states are indicated.

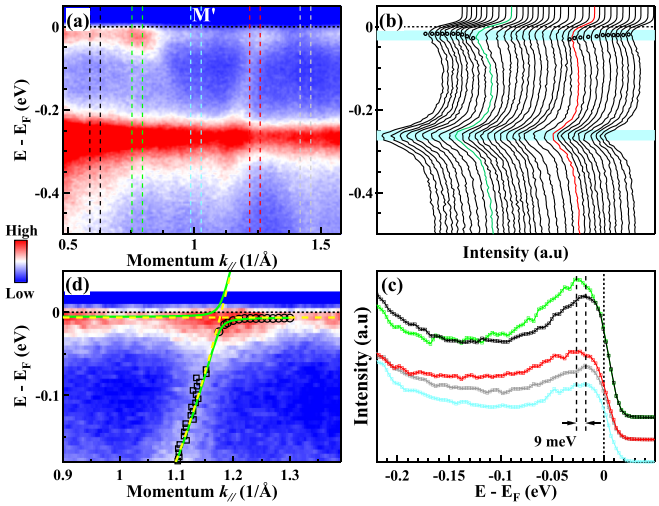


FIG. 4. (**a**) On-resonance valence band structure of $CePd_5Al_2$ measured along a direction slightly off $\Gamma'$-$M'$. (**b**) EDCs of the spectra shown in (a). Aqua shadows indicate $f^1_{5/2}$ and $f^1_{7/2}$ states positions. The open circles indicate EDCs peak positions. (**c and d**) Comparison of EDCs measured at different momentum positions. The black, green, aqua, red, and gray curves were obtained by integrating the regions between two black, green, aqua, red, and gray dashed lines, as indicated in (a), respectively. (**d**) Photoemission intensity near the $E_F$. Squares and open circles represent the conduction and hybridized $f$ bands position, respectively. The hybridized dispersion was fitted by the equation based on the PAM, as indicated by green lines. The horizontal and parabolar yellow-dashed lines represent the $f$-level and the bare conduction band, respectively.

the $f$ band and the conduction band. Thus, we measured high energy resolution on-resonance spectra along the direction slightly deviating from $\Gamma'$-$M'$. The $c$–$f$ hybridization feature is easily detected as shown by the dispersive heavy band near $E_F$ and the redistribution of the $f$-electron spectrum [Fig. 4(a)]. A fraction of the Ce $4f$ electrons are itinerant and involved in FS formation. Note that this is different from a transport measurement viewpoint [16]. Hybridization between $f^1_{5/2}$ and conduction electrons is a common feature in Ce-based HFs [19–22,24,25]. No discernible dispersion was observed for the $4f^1_{7/2}$ state. This may be due to insufficient energy and momentum resolution of the measurement, and that the intensity of the $4f^1_{7/2}$ state is much higher than that of the conduction band.

Figure 4(b) shows the energy distribution curves (EDCs) corresponding to Fig. 4(a). The heavy quasiparticle band peaks near the intersections, indicated by open circles, vary with momentum. Figure 4(c) shows the integrated EDCs at five selected momentum positions shown in different colors in Fig. 4(a). This includes the conduction bands that cross the $E_F$ region and adjacent regions where no conduction bands cross the $E_F$. EDC peak positions in these two regions differ. EDC peak positions in the former regions shift $\sim$ 9 meV toward high-binding energy. This value is similar to that of $CePt_2In_7$ (5 meV) [19] and $CeIn_3$ (4 meV) [21], but significantly smaller than that of $CeIrIn_5$ (about 30 meV) [33]. EDCs peak positions in nonintersecting regions are almost identical (black, aqua, and gray curves). The PAM suggests that, the stronger the $c$–$f$ hybridization, the greater the energy shift in the $f$-level band. This means that the hybridization strength between the $f$ band and the conduction band of $CePd_5Al_2$ is obviously weaker than that of $CeIrIn_5$.

Figure 4(d) presents a zoomed view into the intersections of the $f$ band and the conduction band, and the data have been divided by the corresponding resolution-convoluted Fermi-Dirac function. A weak dispersionless band is observed between the $f$ band and the conduction band intersection. This could be due to the strong Kondo resonance just below $E_F$. The conduction bands represented by the squares and the hybridized $f$ band represented by the open circles were obtained by fitting momentum distribution curves and tracking EDC peak positions, respectively. According to previous work [20,24,30], although $CePd_5Al_2$ is not in a Fermi-Liquid state, its ARPES spectrum can still be analyzed according to the hybridization band picture based on PAM [30,31], in which the hybridization build upper ($E^+$) and lower ($E^-$) bands that are given by

$$E^{\pm}(k) = \frac{\varepsilon_0 + \varepsilon_k \pm \sqrt{(\varepsilon_0 - \varepsilon_k)^2 + 4|V_k|^2}}{2},$$

where $\varepsilon_0$ is the renormalized $f$-level energy (Ce $4f^1_{5/2}$), $\varepsilon_k$ is the bare conduction band, and $V_k$ is the renormalized hybridization (half of the direct hybridization gap) [30]. A good fit result (solid green lines) is achieved [Fig. 4(d)]. This is accomplished by fitting $\varepsilon_0 = -6.2$ meV, and $V_k = 16 \pm 2$ meV. This corresponds to a direct hybridization gap of $\sim$32 meV. This value is similar to that of 30 meV in $CeCoIn_5$ [24] and 36 meV in $CeIrIn_5$ [20]. The indirect gap, obtained by a previous theory calculation, is $\Delta_g \sim 2V_k^2/D$, where $D$ ($D \gg \varepsilon_0$) is the half-bandwidth of the bare conduction band and thus vanishingly small. The fitted results show that the energy spacing between the bottom of the $E^+$ band and the top of the $E^-$ band is quite small. The obtained negative $\varepsilon_0$ value, similar to that of $\gamma$-Ce [32], indicates a ground state $f$ level of $CePd_5Al_2$ has a position just several meV below $E_F$.

To conclude, we investigated the 3D FS topology and the properties of $f$ electrons in the AFM Kondo lattice $CePd_5Al_2$ at low temperatures using high-resolution ARPES. A quasi-2D nature of FSs was detected. Heavy $4f$-derived sharp quasiparticle bands, a strong and sharp $4f^0$ peak at $-1.63$ eV below $E_F$, and spin-orbit splitting of the $4f^1$ final state into $f^1_{7/2}$ and $f^1_{5/2}$ final states were directly observed. Furthermore, a shoulder of the $f^0$ peak, a redistribution of $f^1$ electrons, and a weak dispersive heavy quasiparticle band with an energy shift of $\sim$ 9 meV just below the $E_F$ were observed. The sharp heavy quasiparticle peaks ($f^1_{5/2}$ and $f^1_{7/2}$) near $E_F$ and the hybridized $f$ band indicate that the $f$ electrons are partially itinerant at low temperature, yet dominantly localized. This dual nature of the $4f$ state is derived here from its small but detectable hybridization in $CePd_5Al_2$.

This work was supported by the National Natural Science Foundation of China (Grant Nos. 12074436, 11574402) and the Innovation-driven Plan in Central South University (Grant No. 2016CXS032). J.R. and P.M.O. acknowledge support through the Swedish Research Council (VR) and the Swedish National Infrastructure for Computing (SNIC)

for computing time on computer cluster Triolith at the National Supercomputer Centre Linköping. Y.S. acknowledges the support from the Swedish Research Council (VR) through a Starting Grant (Dnr. 2017-05078). O.T. acknowledges support from the Swedish Research Council (VR) and the Knut and Alice Wallenberg Foundation. M.M. is partly supported by a Marie Sklodowska-Curie Action, International Career Grant through the European Commission and Swedish Research Council (VR), Grant No. INCA-2014-6426, as well as a VR neutron project grant (BIFROST, Dnr. 2016-06955). Further support was also granted by the Carl Tryggers Foundation for Scientific Research (Grants No. CTS-16:324 and No. CTS-17:325). Work at Los Alamos was performed under the auspices of the U.S. Department of Energy, Office of Basic Energy Sciences, Division of Materials Sciences and Engineering.

[1] K. Andres, J. Graebner, and H. Ott, Phys. Rev. Lett. **35**, 1779 (1975).

[2] F. Steglich, J. Aarts, C. D. Bredl, W. Lieke, D. Meschede, W. Franz, and H. Schäfer, Phys. Rev. Lett. **43**, 1892 (1979).

[3] P. Gegenwart, Q. Si, and F. Steglich, Nat. Phys. **4**, 186 (2008).

[4] N. apRoberts-Warren, A. P. Dioguardi, A. C. Shockley, C. H. Lin, J. Crocker, P. Klavins, and N. J. Curro, Phys. Rev. B **81**, 180403(R) (2010).

[5] V. A. Sidorov, M. Nicklas, P. G. Pagliuso, J. L. Sarrao, Y. Bang, A. V. Balatsky, and J. D. Thompson, Phys. Rev. Lett. **89**, 157004 (2002).

[6] Y. F. Xu, C. M. Yue, H. M. Weng, and X. Dai, Phys. Rev. X **7**, 011027 (2017).

[7] C. Y. Guo, F. Wu, Z. Z. Wu, M. Smidman, C. Cao, A. Bostwick, C. Jozwiak, E. Rotenberg, Y. Liu, F. Steglich, and H. Q. Yuan, Nat. Commun. **9**, 4622 (2018).

[8] C. Cao, G. X. Zhi, and J. X. Zhu, Phys. Rev. Lett **124**, 166403 (2020).

[9] D. Aoki, Y. Haga, T. D. Matsuda, N. Tateiwa, S. Ikeda, Y. Homma, H. Sakai, Y. Shiokawa, E. Yamamoto, A. Nakamura, R. Settai, and Y. Ōuki, J. Phys. Soc. Jpn. **76**, 063701 (2007).

[10] Y. Haga, D. Aoki, Y. Homma, S. Ikeda, T. D. Matsuda, E. Yamamoto, H. Sakai, N. Tateiwa, N. D. Dung, A. Nakamura, Y. Shiokawa, and Y. Ōnuki, J. Alloys Compd. **464**, 47 (2008).

[11] R. A. Ribeiro, Y. F. Inoue, T. Onimaru, M. A. Avila, K. Shigetoh, and T. Takabatake, Physica B **404**, 2946 (2009).

[12] R. A. Ribeiro, T. Onimaru, K. Umeo, M. de Abreu Avila, K. Shigetoh, and T. Takabatake, J. Phys. Soc. Jpn. **76**, 123710 (2007).

[13] F. Honda, M. A. Measson, Y. Nakano, N. Yoshitani, E. Yamamoto, Y. Haga, T. Takeuchi, H. Yamagami, K. Shimizu, R. Settai, and Y. Ōnuki, J. Phys. Soc. Jpn. **77**, 43701 (2008).

[14] Y. F. Inoue, T. Onimaru, A. Ishida, T. Takabatake, Y. Oohara, T. J. Sato, D. T. Adroja, A. D. Hillier, and E. A. Goremychkin, J. Phys. Conf. Ser. **200**, 32023 (2010).

[15] T. Onimaru, Y. F. Inoue, A. Ishida, K. Umeo, Y. Oohara, T. J. Sato, D. T. Adroja, and T. Takabatake, J. Phys. Condens. Matter **31**, 125603 (2019).

[16] T. Onimaru, Y. F. Inoue, K. Shigetoh, K. Umeo, H. Kubo, R. A. Ribeiro, A. Ishida, M. A. Avila, K. Ohoyama, M. Sera, and T. Takabatake, J. Phys. Soc. Jpn. **77**, 074708 (2008).

[17] Y. Nakano, F. Honda, T. Takeuchi, K. Sugiyama, M. Hagiwara, K. Kindo, E. Yamamoto, Y. Haga, R. Settai, H. Yamagami, and Y. Ōnuki, J. Phys. Soc. Jpn. **79**, 024702 (2010).

[18] See Supplemental Material at http://link.aps.org/supplemental/10.1103/PhysRevB.103.125122 for band structures of $CePd_5Al_2$ with different photon energies, and calculation of $f^1$-to-$f^0$ ratio.

[19] Y. X. Duan, C. Zhang, J. Rusz, P. M. Oppeneer, T. Durakiewicz, Y. Sassa, O. Tjernberg, M. Månsson, M. H. Berntsen, F. Y. Wu, Y. Z. Zhao, J. J. Song, Q. Y. Wu, Y. Luo, E. D. Bauer, J. D. Thompson, and J. Q. Meng, Phys. Rev. B **100**, 085141 (2019).

[20] Q. Y. Chen, C. H. P. Wen, Q. Yao, K. Huang, Z. F. Ding, L. Shu, X. H. Niu, Y. Zhang, X. C. Lai, Y. B. Huang, G. B. Zhang, S. Kirchner, and D. L. Feng, Phys. Rev. B **97**, 075149 (2018).

[21] Y. Zhang, W. Feng, X. Lou, T. Yu, X. Zhu, S. Tan, B. Yuan, Yi. Liu, H. Lu, D. Xie, Q. Liu, W. Zhang, X. Luo, Y. Huang, L. Luo, Z. Zhang, X. Lai, and Q. Chen, Phys. Rev. B **97**, 045128 (2018).

[22] S. Patil, A. Generalov, M. Güttler, P. Kushwaha, A. Chikina, K. Kummer, T. C. Rödel, A. F. Santander-Syro, N. Caroca-Canales, C. Geibel, S. Danzenbächer, Yu. Kucherenko, C. Laubschat, J. W. Allen, and D. V. Vyalikh, Nat. Commun. **7**, 11029 (2016).

[23] J. W. Allen, S. J. Oh, O. Gunnarsson, K. Schönhammer, M. B. Maple, M. S. Torikachvili, and I. Lindau, Adv. Phys. **35**, 275 (1986).

[24] Q. Y. Chen, D. F. Xu, X. H. Niu, J. Jiang, R. Peng, H. C. Xu, C. H. P. Wen, Z. F. Ding, K. Huang, L. Shu, Y. J. Zhang, H. Lee, V. N. Strocov, M. Shi, F. Bisti, T. Schmitt, Y. B. Huang, P. Dudin, X. C. Lai, S. Kirchner, H. Q. Yuan, and D. L. Feng, Phys. Rev. B **96**, 045107 (2017).

[25] H. Liu, Y. Xu, Y. Zhong, J. Guan, L. Kong, J. Ma, Y. Huang, Q. Chen, G. Chen, M. Shi, Y. Yang, and H. Ding, Chin. Phys. Lett. **36**, 097101 (2019).

[26] Y. Luo, C. Zhang, Q. Y. Wu, F. Y. Wu, J. J. Song, W. Xia, Y. F. Guo, J. Rusz, P. M. Oppeneer, T. Durakiewicz, Y. Z. Zhao, H. Liu, S. X. Zhu, Y. H. Yuan, X. F. Tang, J. He, S. Y. Tan, Y. B. Huang, Z. Sun, Y. Liu, H. Y. Liu, Y. X. Duan, and J. Q. Meng, Phys. Rev. B **101**, 115129 (2020).

[27] S.-I. Fujimori, Y. Saitoh, T. Okane, A. Fujimori, H. Yamagami, Y. Haga, E. Yamamoto, and Y. Onuki, Nat. Phys. **3**, 618 (2007).

[28] J. Q. Meng, P. M. Oppeneer, J. A. Mydosh, P. S. Riseborough, K. Gofryk, J. J. Joyce, E. D. Bauer, Y. Li, and T. Durakiewicz, Phys. Rev. Lett. **111**, 127002 (2013).

[29] J. J. Yeh and I. Lindau, At. Data Nucl. Data Tables **32**, 1 (1985).

[30] H. J. Im, T. Ito, H. D. Kim, S. Kimura, K. E. Lee, J. B. Hong, Y. S. Kwon, A. Yasui, and H. Yamagami, Phys. Rev. Lett. **100**, 176402 (2008).

[31] P. Coleman, Heavy electrons, in *Introduction to Many-Body Physics* (Cambridge University Press, Cambridge, 2010), pp. 656–719.

[32] X. Zhu, Y. Liu, Y. Zhao, Y. Wang, Y. Zhang, C. Lu, Y. Duan, D. Xie, W. Feng, D. Jian, Y. Wang, S. Tan, Q. Liu, W. Zhang, Y. Liu, L. Luo, X. Luo, Q. Chen, H. Song, and X. Lai, npj Quant. Mater. **5**, 47 (2020).

[33] S. I. Fujimori, A. Fujimori, K. Shimada, T. Narimura, K. Kobayashi, H. Namatame, M. Taniguchi, H. Harima, H. Shishido, S. Ikeda, D. Aoki, Y. Tokiwa, Y. Haga, and Y. Ōnuki, Phys. Rev. B **73**, 224517 (2006).